Discrete-Time Domain Modeling of a High-Power Medium-Voltage Resonant Converter

Mahdizadeh Shalmaei, Amir Hossein; N. Soltani, Mohsen; Hajizadeh, Amin

Published in:
2023 25th European Conference on Power Electronics and Applications, EPE 2023 ECCE Europe

DOI (link to publication from Publisher):
10.23919/EPE23ECCEEurope58414.2023.10264296

Publication date:
2023

Document Version
Accepted author manuscript, peer reviewed version

Discrete-Time Domain Modeling of a High-Power Medium-Voltage Resonant Converter

Amir Hossein Mahdizadeh, Mohsen Soltani, and Amin Hajizadeh
Aalborg University / AAU Energy
Esbjerg, Denmark
Tel.: +45-52687875.

{ahms, sms, aha}@energy.aau.dk

ACKNOWLEDGEMENT

This work was partially supported by AAU Energy, EUDP project no. 640222-496821, and Energy Cluster Denmark under project W-Tools. Furthermore, the Authors would like to thank Dr. Catalin Gabriel Dincan from Vestas Wind Systems A/S, Denmark for providing invaluable inputs.

***Index Terms*—Medium voltage DC-DC converter, LLC resonant converter, Modelling, Discrete-time domain analysis**

***Abstract*—LLC resonant converters are widely used in diverse industrial applications, due in part to their high efficiency and high power density. In spite of their numerous advantages, these converters are still considered the most challenging converters from a modeling and control perspective. Several factors contribute to this complexity, including the nonlinear behavior and different operating modes. Therefore, a high-power medium-voltage resonant converter is modeled in this manuscript, and its dynamic behavior is investigated. The nonlinear model simulation performed by MATLAB/Simulink and the electrical circuit simulation performed by PLECS are then compared to verify the accuracy of the obtained model.**

I. INTRODUCTION

High-power Medium-voltage DC-DC (MVDC) converters have attracted considerable attention in renewable energy applications, such as offshore wind farms, where MVDC converters are used to raise the renewably generated voltage to medium levels as depicted in Fig. 1. Among the diverse types of DC-DC converters, the Series-LLC Resonant Converter (SRC), shown in Fig. 2, is one of the most appealing ones as it offers unique attributes. Power density and efficiency are critical factors. Another notable feature is the ability to switch softly on both the inverter and rectifier sides [1], [2]. Furthermore, due to its Zero Voltage Switching (ZVS) and Zero Current Switching (ZCS) properties, this converter has low Electro-Magnetic Interference (EMI) [3].

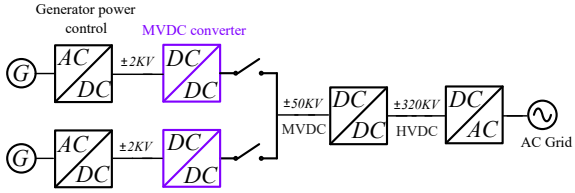

Fig. 1. Single line schematic of a DC wind farm.

However, this converter has its own shortcomings when it comes to modeling and control; namely, unlike converters operating on Pulse-Width Modulation (PWM), where the small signal analysis is well established, obtaining a unique model describing the SRC behavior is more challenging [4], [5]. There have been several approaches proposed to date. In [6], a modified method for deriving the model of the SRC is presented. The foundation of this strategy is communication theory, through which a control-to-output transfer function is obtained. One of the main drawbacks of this approach is the low model accuracy for lower frequencies. The Virtual Network Analyzer (VNA) approach presented by [7] measures the transfer function of a device under test. The accuracy of this method is high, but the simulation time is quite long as repetition of the procedure for various switching frequencies is necessary. As suggested by [7], sampled-data modeling is very fast but offers less accuracy at higher frequencies. Meanwhile, as far as the operating modes of the converter increase, extremely analytical and numerical efforts would be essential. Modeling that relies on First Harmonic Approximation (FHA) is another approach proposed by [8]. Even though modeling based on this method is accurate when the converter operates at the resonant frequency, accuracy diminishes as long as the switching frequency deviates

from the resonant frequency. Modeling based on the Extended Describing Function (EDF) method is suggested by [9] and [10] to address the inaccuracy issue caused by frequency deviations. In this strategy, the Fourier series approximates the nonlinear behavior of different elements. This approach is tedious because new small-signal equivalent circuits are needed for nonlinear elements. Another way to obtain the dynamic model of the converter is called Discrete-Time Domain Modeling, proposed by [11]. The concept behind this method is calculating state variables at the beginning of each switching cycle. This idea was later developed and employed for a pulse-removal-technique-driven SRC [12]. But neither the model's dynamic behavior is thoroughly analyzed, nor is the control input chosen according to the obtained transfer function.

Hence, the main contribution of this manuscript is to apply the discrete-time domain modeling method to the SRC to provide better information on the nonlinearities of the LLC tank. The dynamic and static behaviors of the nonlinear models are investigated under different circumstances and then compared with the converter simulation results.

This manuscript is organized as follows: the large-signal analysis of the SRC is conducted in section (II). After that, the small-signal analysis is given in section (III), and the conclusion is provided in section (IV).

II. Large Signal Analysis of the Converter

As shown in Fig. 2, the converter consists of a full-bridge inverter, a high-frequency transformer with N1 and N2 turns for the primary and secondary windings, a resonant tank containing a resonant inductor, a resonant capacitor, and a full-bridge medium-voltage rectifier. This converter operates in three distinct modes, namely sub-resonant, resonant, and super-resonant, of which the sub-resonant mode is the subject of this paper. The sub-resonant mode is most efficient in terms of power and size because of the natural commutation of the switches that occurs while the switches are turned off. This, in turn, results in less switching loss and higher efficiency, which is attractive for high-power applications. Furthermore, this mode of operation can also maintain a constant output voltage in cases of varying input voltages. Sub-resonant mode occurs when the switching frequency (f_s) is less than the natural frequency (f_r) obtained from the resonant tank parameters. Hence, should the converter operate in sub-resonant mode, the mean output power becomes a function of the number of current pulses transmitted to the load [12]. The switch pairs (S_1, S_4) and (S_2, S_3) in Fig. 3 are triggered complementarily with a %50 duty cycle. Following that, the transformer levels up the inverter's square wave voltage to the desired magnitude before exciting the resonant tank. After being rectified by the full-bridge rectifier, the resonant current feeds the medium-voltage direct current (MVDC) network. Since the equivalent circuits of the converter for the switch pairs (S_1, S_4) and (S_2, S_3) are symmetrical, the mathematical equations are derived using only half of a whole periodic operation. When the switch pair (S1, S4) conducts, the converter operates in two modes, as shown in Fig. 2 and Fig. 3, which are detailed in detail below.

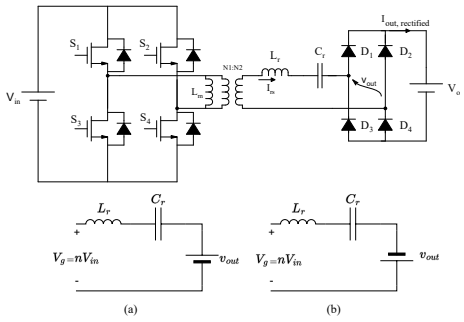

Fig. 2. Basic schematic of an LLC resonant converter; (a) equivalent circuit in the first mode of operation, and (b) equivalent circuit in the second mode of operation

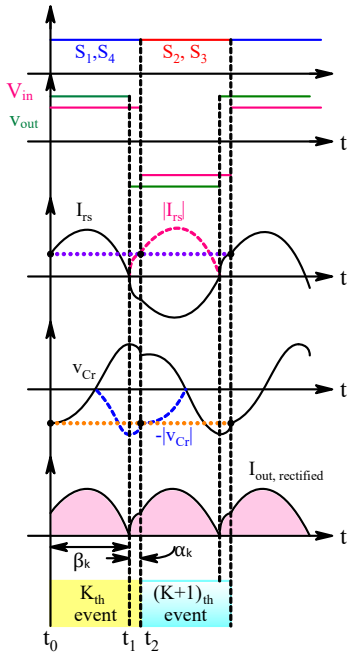

Fig. 3. Key wave forms of the converter.

Time interval $[t_0\ t_1]$: this mode of operation initiates when the switches (S_1, S_4) conduct. Hence, the input

voltage is applied to the resonant tank, and a sinusoidal resonant current flows through the resonant tank. Since the converter operates in the capacitive region, the resonant current waveform leads the capacitor voltage waveform, as depicted in Fig. 3. This mode of operation ends when the sinusoidal current reaches zero and provides ZCS condition for the switches (S_1, S_4). Mathematical equations describing the converter dynamics related to this time interval are:

$$V_g = L_r \frac{dI_{rs}(t)}{dt} + v_{Cr}(t) + v_{out}(t), \tag{1}$$

$$I_{rs}(t) = C_r \frac{dv_{Cr}(t)}{dt}. \tag{2}$$

It is noted that $I_{rs}(t)$, $v_{Cr}(t)$, and $v_{out}(t)$ are, respectively, the resonant current in the secondary side of the transformer, the resonant voltage across the resonant capacitor, and the voltage applied to the rectifier. V_g also stands for DC input voltage. The solutions to differential equations (1) and (2) are:

$$I_{rs}(t) = \frac{V_g - v_{Cr0} - v_{out}}{z_r} sin(w_r t) + I_{rs0} cos(w_r t), \tag{3}$$

$$\begin{aligned} v_{Cr}(t) = &- (V_g - v_{Cr0} - v_{out}) cos(w_r t) \\ &+ I_{rs0} z_r sin(w_r t) + V_g - v_{out}, \end{aligned} \tag{4}$$

$$w_r = \frac{1}{\sqrt{L_r C_r}}, \tag{5}$$

$$z_r = \sqrt{\frac{L_r}{C_r}}, \tag{6}$$

where I_{rs0} and v_{Cr0} are the initial inductor current and initial capacitor voltage, respectively. Also, w_r denotes the resonant frequency. In addition, z_r represents the characteristic impedance of the resonant tank. As this mode of operation ends when the resonant current reaches zero, the time when zero crossing occurs could be obtained as follows:

$$t_1 = \frac{1}{w_r} \left[tan^{-1}\left(\frac{-I_{rs0} z_r}{V_g - v_{out} - v_{Cr0}}\right) + \pi \right]. \tag{7}$$

As stated in equation (8), the time interval of this state is β.

$$\beta = t_1 - t_0. \tag{8}$$

Time interval [t_1 t_2]: this mode of operation starts when the negative resonant current passes through the anti-parallel diodes of the switches (S_1, S_4). The differential equations derived from the equivalent circuit during this time interval are presented:

$$\begin{aligned} V_g &= L_r \frac{dI_{rs}(t)}{dt} + v_{Cr}(t) - v_{out}, \\ I_{rs}(t) &= -C_r \frac{dv_{Cr}(t)}{dt}. \end{aligned} \tag{9}$$

Thus, similar to what was stated for the period [t_0 t_1], the inductor current and the capacitor voltage are obtained.

$$\begin{aligned} I_{rs}(t) = &(2v_{out} + (V_g - v_{Cr0} - v_{out}) cos(w_r t_1) \\ &- I_{rs0} z_r sin(w_r t_1)) \frac{1}{z_r} sin(w_r t), \end{aligned} \tag{10}$$

$$\begin{aligned} v_{cr}(t) = &V_g + v_{out} + (-2v_{out} - (V_g - v_{out} - v_{Cr0}) \\ &cos(w_r t_1) + I_{rs0} z_r sin(w_r t_1)) cos(w_r t). \end{aligned} \tag{11}$$

This mode of operation ends when the other switch pair is activated. It is worth mentioning that the duration of this time interval, defined as α, is:

$$\alpha = \frac{1}{2f_s} - \beta, \tag{12}$$

where f_s is the switching frequency.

As these equations merely describe the behavior of the resonant tank, the need for the third equation in terms of the input (f_s) and the output $I_{out,rec}$ is essential. For this purpose, the effect of the output filter is neglected due to its slow dynamic compared to that of the resonant tank. Instead, only the DC component of the rectified output current is considered. Regarding the rectified output current depicted in Fig. 3, the average value could be calculated as follows:

$$\begin{aligned} I_{out,rec} = &\frac{1}{\gamma} \left(\int_0^{\beta} I_{rs}(t) dt + \int_0^{\alpha} I_{rs}(t) dt \right) \\ = &\frac{1}{\gamma} \{ [\frac{-1}{z_r} (V_g - v_{Cr0} - v_{out})(cos(w_r \beta) - 1) \\ &+ I_{rs0} sin(w_r \beta)] + \frac{1}{z_r} [2v_{out} + (V_g - v_{Cr0} \\ &- v_{out}) cos(w_r \beta) - I_{rs0} z_r sin(w_r \beta)] \\ &(cos(w_r \alpha) - 1)) \}. \end{aligned} \tag{13}$$

In this equation, γ is the duration in which the switch pair (S_1, S_4) conducts.

$$\gamma = \alpha + \beta. \tag{14}$$

This time interval is later defined as an "event" being repeated when each switch pair conducts.

III. Small Signal Analysis

In Fig. 3, the event starting at t_0 and ending at t_2 is referred to as the $(k)_{th}$ event. As can be seen, the endpoints of the $(k)_{th}$ event are equal to the start points of the $(k+1)_{th}$ event; therefore, these values are potential candidates for forming discrete state variables.

$$\begin{aligned} x_1 = I_{rs,0(k)} = -I_{rs,0(k+1)} = I_{rs0}, \\ x_2 = v_{Cr,0(k)} = -v_{C_r,0(k+1)} = v_{Cr0}. \end{aligned} \tag{15}$$

Given these equations, the capacitor voltage and the inductor current are expressed by $V_{C_r,j(k)}$ and $I_{rs,j(k)}$ where subscripts k and j, respectively, denote the $(k)_{th}$ event and a specific time within the event as mentioned earlier. Based on what was expressed, the continuous model of the converter presented in the previous section could be converted to a discrete model only describing the start points and the endpoints.

$$\begin{aligned} I_{rs,2(k)} = [2v_{out,0(k)} + (V_{in,0(k)} - v_{Cr,0(k)} - v_{out,0(k)}) \\ cos(w_r\beta) - I_{rs,0(k)} z_r sin(w_r\beta)] \frac{1}{z_r} sin(w_r\alpha), \end{aligned} \tag{16}$$

$$\begin{aligned} v_{cr,2(k)} =& [-2v_{out,0(k)} - (V_{g,0(k)} - v_{out,0(k)} \\ & - v_{Cr,0(k)}) cos(w_r\beta) + I_{rs0} z_r sin(w_r\beta)] \\ & cos(w_r\alpha) + V_{g,0(k)} + v_{out,0(k)}, \end{aligned} \tag{17}$$

$$V_{in,0(k)} = V_g, V_{out,0(k)} = V_o, \tag{18}$$

where $I_{rs,2(k)}$ and $v_{cr,2k}$ define the values for the inductor current and the capacitor voltage at t_2. This, in turn, leads the continuous mathematical equations (10) and (11) to be only two points at the time t_2 , as shown in Fig. 3.

Connecting the starting points and endpoints, shown in Fig. 3, the lines are used to convert the single discrete points into a continuous waveform. As can be seen in this figure, the discrete model could be converted to a continuous time-based model by the derivative definition, which is:

$$\dot{x} = \frac{x_{i(k+1)} - x_{i(k)}}{t_{i(k+1)} - t_{i(k)}}. \tag{19}$$

Substituting equations (16) and (17) into equation (19) and taking equation (15) into account results in nonlinear state equations which are:

$$\begin{aligned} \dot{x_1} =& 2f_s\{[sin(w_r\beta)sin(w_r\alpha) - 1]x_1 \\ & + [sin(w_r\alpha)cos(w_r\beta)]\frac{x_2}{z_r} \\ & + [-2sin(w_r\alpha) + cos(w_r\beta)sin(w_r\alpha)]\frac{v_{out,0(k)}}{z_r} \\ & + [-cos(w_r\beta)sin(w_r\alpha)]\frac{V_{g,0(k)}}{z_r}\} \\ =& f_1(x_1, x_2, f_s, V_{g,0(k)}, v_{out,0(k)}) \\ =& f_1(x_1, x_2, V_g, v_{out}), \end{aligned} \tag{20}$$

$$\begin{aligned} \dot{x_2} =& 2f_s\{[z_r sin(w_r\beta)cos(w_r\alpha)]x_1 \\ & + [cos(w_r\beta)cos(w_r\alpha) + 1]x_2 \\ & + [-2cos(w_r\alpha) + cos(w_r\alpha)cos(w_r\beta) + 1]v_{out,0(k)} \\ & + [-cos(w_r\alpha)cos(w_r\beta) + 1]V_{g,0(k)}\} \\ =& f_2(x_1, x_2, f_s, V_{g,0(k)}, v_{out,0(k)}) \\ =& f_2(x_1, x_2, V_g, v_{out}). \end{aligned} \tag{21}$$

Similarly, the average rectified output current given in equation (13) follows the same format as equations (16) and (17) provided that the notations expressed in equation (15) are used.

$$\begin{aligned} I_{out,rec} =& \frac{1}{\gamma}\{[\frac{-1}{z_r}(V_{g,0(k)} - x_2 - v_{out,0(k)}) \\ & (cos(w_r\beta) - 1)) + x_1 sin(w_r\beta)] \\ & + \frac{1}{z_r}[2v_{out,0(k)} + (V_{g,0(k)} - x_2 - v_{out,0(k)}) \\ & cos(w_r\beta) - x_1 z_r sin(w_r\beta)](cos(w_r\alpha) - 1))\} \\ =& f_3(x_1, x_2, V_{g,0(k)}, v_{out,0(k)}) \\ =& f_3(x_1, x_2, V_g, v_{out}). \end{aligned} \tag{22}$$

TABLE I
Parameter specifications [2].

Nominal power	10 MW
Nominal input Voltage (V_g)	2 kV
Nominal output Voltage (V_o)	50 kV
Resonant inductor (L_r)	78.1 mH
Resonant capacitor (C_r)	0.25 μF
Magnetizing inductance (L_m)	10 mH
Nominal switching frequency (f_s)	1000 Hz
Range of switching frequency deviation	$\pm$100 Hz
n	25

The phase plane of the nonlinear system with the specifications provided in table I for different fixed values of switching frequencies is depicted in Fig. 4. Based

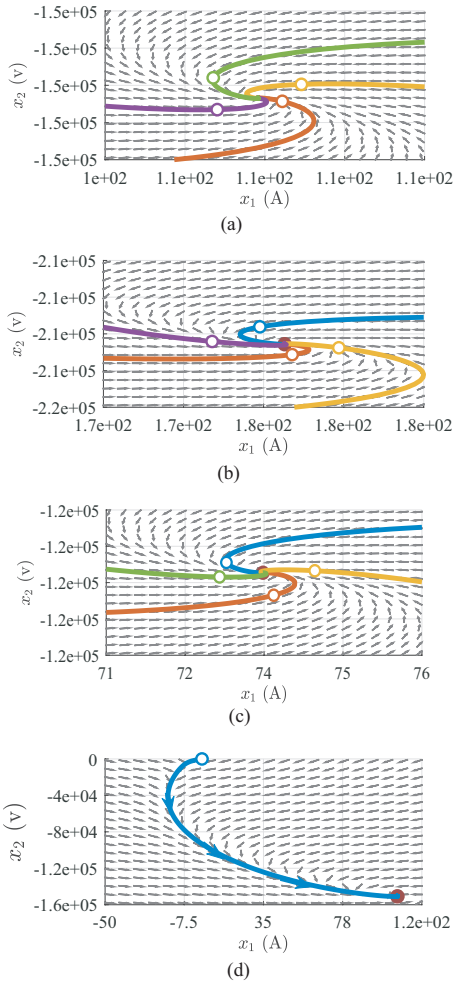

Fig. 4. Global qualitative behavior of the system for the frequencies:(a) 1000 Hz and the equilibrium point is (106 A,-150 kV) ,(b) 1050 Hz, and the equilibrium point is (176 A, -210 kV),(c) 950 Hz and the equilibrium point is (73 A, -120 kV)(d) the state trajectory of the system for 1000 Hz and zero initial condition.

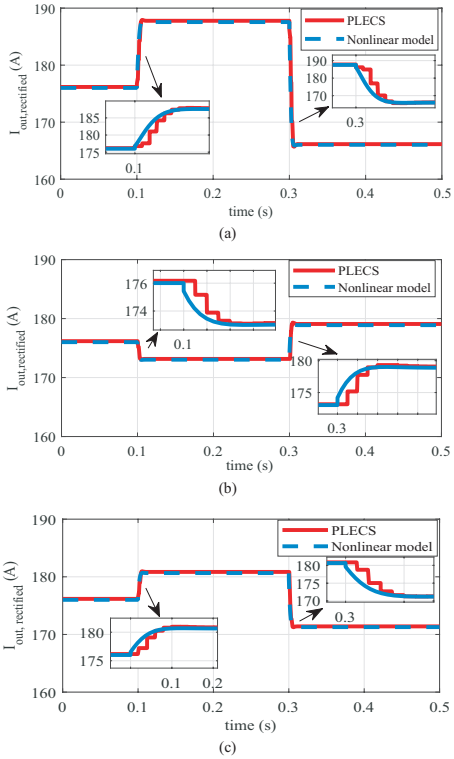

Fig. 5. Comparison of the results derived from the obtained nonlinear model simulated by Simulink/MATLAB and the circuit simulated by PLECS for (a) different fixed switching frequencies, (b) different fixed output voltages and (c) different fixed input voltages.

on a practical investigation, the only equilibrium point in the converter's feasible operating range is as shown in Fig. 4. As can be seen, the circles are randomly chosen points through which the trajectories pass and they do not carry any significant information. The examination of these phase portraits demonstrates that the trajectories approach and finally reach a single point, known as the trim point no matter what the states' initial values are; To illustrate further, trajectories with different colors are related to the dynamical behaviors of the system for various initial values of the states. Meanwhile, the trajectories in the vicinity of the equilibrium point form an attractive focus point that implies the system stability. Moreover, this stable focus point shows that the open-loop system should possess underdamped behavior to a step input. Another important attribute of this converter is revealed if the phase portraits illustrated in Fig. 4(a), Fig. 4(b), and Fig. 4(c) are compared. As it is apparent, the values for the equilibrium point change when the switching frequency varies; that is, the topological or qualitative behavior of the system changes. This means that the system's characteristic includes a bifurcation behavior. Meanwhile, it is worth noting that the trajectory approaches the equilibrium point even if the states' initial conditions are considered zero as shown in Fig. 4. Given that all the state variables defined in equations (20) and (21) are close enough to an equilibrium point, the nonlinear state equations could be linearized around the operating point through the Jacobian matrix.

The nonlinear model results are compared to the simulated converter results to verify the validity of the preceding analysis. For this purpose, %1 step perturbation is separately applied to the three inputs. Then, the simulated nonlinear model results obtained by Simulink/MATLAB are compared with those of the simulated converter conducted by PLECS software. As shown in Fig. 5(a), the nonlinear model of the SRC witnesses nearly the same dynamic and static behaviors

as the circuit simulated by PLECS does when the nominal frequency deviates by %1. The same comparative analysis is as well conducted when the step perturbations are applied to v_{out} and V_{in} as illustrated in Fig. 5(b) and Fig. 5(c). The evaluation of these figures confirms the validity of the nonlinear discrete-time domain model as the dynamic and static behaviors of the output current obtained by the nonlinear model are consistent with that of the rectified output current obtained via PLECS.

IV. Conclusion

In this study, the nonlinear model of an SRC is obtained through discrete-time domain modeling. The converter's qualitative behavior for different switching frequencies is evaluated by phase portrait. The nonlinear model is simulated by Simulink/Matlab and the results are compared to those of the converter simulated by PLECS. Based on this examination, the nonlinear model's accuracy is confirmed. With respect to the analysis, it also becomes clear that the SRC shows a bifurcation effect. This is why the need for a nonlinear controller, such as a gain scheduling controller, is justified to ensure consistent performance over a wide range of switching frequencies.

References

[1] C. Dincan, P. Kjaer, Y. -h. Chen, S. Munk-Nielsen and C. L. Bak, "Analysis of a High-Power, Resonant DC–DC Converter for DC Wind Turbines," in IEEE Transactions on Power Electronics, vol. 33, no. 9, pp. 7438-7454, Sept. 2018, doi: 10.1109/TPEL.2017.2770322.

[2] C. G. Dincan et al., "Design of a High-Power Resonant Converter for DC Wind Turbines," in IEEE Transactions on Power Electronics, vol. 34, no. 7, pp. 6136-6154, July 2019, doi: 10.1109/TPEL.2018.2876320.

[3] L. A. D. Ta, N. D. Dao and D. -C. Lee, "High-Efficiency Hybrid LLC Resonant Converter for On-Board Chargers of Plug-In Electric Vehicles," in IEEE Transactions on Power Electronics, vol. 35, no. 8, pp. 8324-8334, Aug. 2020, doi: 10.1109/TPEL.2020.2968084.

[4] F. Degioanni, I. G. Zurbriggen and M. Ordonez, "Dual-Loop Controller for LLC Resonant Converters Using an Average Equivalent Model," in IEEE Transactions on Power Electronics, vol. 33, no. 11, pp. 9875-9889, Nov. 2018, doi: 10.1109/TPEL.2017.2786044.

[5] M. Mohammadi, F. Degioanni, M. Mahdavi and M. Ordonez, "Small-Signal Modeling of LLC Converters Using Homopolarity Cycle," in IEEE Transactions on Power Electronics, vol. 35, no. 4, pp. 4076-4093, April 2020, doi: 10.1109/TPEL.2019.2933179.

[6] B. Cheng, F. Musavi and W. G. Dunford, "Novel small signal modeling and control of an LLC resonant converter," 2014 IEEE Applied Power Electronics Conference and Exposition - APEC 2014, Fort Worth, TX, USA, 2014, pp. 2828-2834, doi: 10.1109/APEC.2014.6803705.

[7] J. Stahl, T. Hieke, C. Oeder and T. Duerbaum, "Small signal analysis of the resonant LLC converter," 2013 IEEE ECCE Asia Downunder, Melbourne, VIC, Australia, 2013, pp. 25-30, doi: 10.1109/ECCE-Asia.2013.6579069.

[8] T. Duerbaum, "First harmonic approximation including design constraints," INTELEC - Twentieth International Telecommunications Energy Conference (Cat. No.98CH36263), San Francisco, CA, USA, 1998, pp. 321-328, doi: 10.1109/INTLEC.1998.793519

[9] C. -H. Chang, E. -C. Chang, C. -A. Cheng, H. -L. Cheng and S. -C. Lin, "Small Signal Modeling of LLC Resonant Converters Based on Extended Describing Function," 2012 International Symposium on Computer, Consumer and Control, Taichung, Taiwan, 2012, pp. 365-368, doi: 10.1109/IS3C.2012.99.

[10] S. Tian, F. C. Lee and Q. Li, "Equivalent circuit modeling of LLC resonant converter," 2016 IEEE Applied Power Electronics Conference and Exposition (APEC), Long Beach, CA, USA, 2016, pp. 1608-1615, doi: 10.1109/APEC.2016.7468082.

[11] R.J. King, and T.A. Stuart, "Small-signal model for the series resonant converter," in IEEE transactions on aerospace and electronic systems, no. 3, 1985, pp.301-319.

[12] Y.H. Chen, C.G. Dincan, P. Kjær, C.L. Bak, X. Wang, C.E. Imbaquingo, E. Sarrà, N. Isernia, and A. Tonellotto, "Model-based control design of series resonant converter based on the discrete time domain modeling approach for DC wind turbine," in Journal of Renewable Energy, 2018, pp.1-18.